Jig-Shape Optimization of a Low-Boom Supersonic Aircraft

Chan-gi Pak[1]
NASA Armstrong Flight Research Center, Edwards, CA 93523-0273

A simple approach for optimizing the jig-shape is proposed in this study. This simple approach is based on an unconstrained optimization problem and applied to a low-boom supersonic aircraft. In this study, the jig-shape optimization is performed using the two-step approach. First, starting design variables are computed using the least-squares surface fitting technique. Next, the jig-shape is further tuned using a numerical optimization procedure based on an in-house object-oriented optimization tool. During the numerical optimization procedure, a design jig-shape is determined by the baseline jig-shape and basis functions. A total of 12 symmetric mode shapes of the cruise-weight configuration, rigid pitch shape, rigid left and right stabilator rotation shapes, and a residual shape are selected as sixteen basis functions. After three optimization runs, the trim shape error distribution is improved, and the maximum trim shape error of 0.9844 inches of the starting configuration becomes 0.00367 inch by the end of the third optimization run.

Acronyms

CG = center of gravity
FE = finite element
HSCT = high-speed civil transport
LMSW = Lockheed Martin Skunk Works
O^3 = object-oriented optimization
PLdB = perceived loudness in decibels

Nomenclature

$F(X)$ = objective function
ndv = number of design variables
ngrid×3 = number of grid points times three
nsurf×3 = number of surface grid points times three
Nx = translational acceleration along x axis
Ny = translational acceleration along y axis
Nz = translational acceleration along z axis
P = roll velocity
Pdot = roll acceleration
Q = pitch velocity
Qdot = pitch acceleration
R = yaw velocity
Rdot = yaw acceleration
ΔT_j = j-th element of the vector $\{\Delta T\}$
X_i = i-th design variable, i=1, 2, …, ndv
X_i^L = lower bound of the i-th design variable X_i, i=1, 2, …, ndv
X_i^U = upper bound of the i-th design variable X_i, i=1, 2, …, ndv
$\alpha_{Flexible}$ = angle of attack using a flexible structure assumption

[1] Senior Aerospace Engineer, Aerostructures Branch, P.O. Box 273, Edwards, California / Mail Stop 48201A, Senior Member AIAA.

α_{Rigid} = angle of attack using a rigid structure assumption
$\{jig\}_b$ = baseline jig-shape
$\{jig\}_d$ = design jig-shape
$\{\Delta jig\}$ = jig-shape changes
$\{\Delta T\}$ = trim shape error based on the design jig-shape
$\{\Delta T\}_t$ = trim shape error based on the baseline jig-shape
$\{\Delta T\}_i$ = i-th shape function, i=1, 2, …, ndv
$\{T\}_b$ = trim shape based on the baseline jig-shape
$\{T\}_d$ = trim shape based on the design jig-shape
$\{T\}_i$ = i-th trim shape based on the i-th basis function, i=1, 2, …, ndv
$\{T\}_t$ = target trim shape
$\{\phi\}_i$ = i-th basis function, i=1, 2, …, ndv
$\{X\}$ = design variable vector $\{X\} = \lfloor X_1, X_2, \ldots, X_{ndv} \rfloor^T$
$[\boldsymbol{\Phi}]$ = basis matrix $[\boldsymbol{\Phi}] = [\{\phi\}_1 \{\phi\}_2 \ldots \{\phi\}_{ndv}]$
$[\boldsymbol{\Psi}]$ = shape matrix $[\boldsymbol{\Psi}] = [\{\Delta T\}_1 \{\Delta T\}_2 \ldots \{\Delta T\}_{ndv}]$

I. Introduction

The impact of aeroelastic effects on a high-speed civil transport (HSCT) aircraft design have been discussed in the previous research [1]. During a conceptual design study of a low-boom aircraft [2], it has been reported that one degree of the tip twist for the low-boom aircraft wing and stabilator under the cruise flight condition could increase the sonic boom level by 0.2 PLdB and 1.3 PLdB, respectively. An accurate aeroelastic trim shape for a low-boom aircraft under cruise flight condition therefore is essential for future low-boom aircraft, including jig-shape optimization during the design to ensure a minimum error between the computed aeroelastic trim shape and target trim shape, on which the computation of sonic boom level is based.

Jig-shape optimization is one popular application of combined aerodynamic and structural optimization. First, the outer-mold-line configuration of an aircraft is designed for the desired aerodynamic performance. Aerodynamic loads computed using the outer-mold-line configuration, however, can cause structural deformation due to the flexibility of the structure. These structural deformations then change the aircraft configuration for the aerodynamic load computation, affecting the structural deformation once again. A paper by Sobieski and Haftka [3] provides a survey of combined aerodynamic and structural optimization. A jig-shape optimization of an HSCT wing was performed by Rohl et al. [4] using a simultaneous aerodynamic and structural optimization procedure. Their optimum wing twist and camber distribution is designed using WINGDES code [5], based on a linearized potential flow solver. The structural optimization of the HSCT wing box structure was performed using automated structural optimization system (ASTROS) code [6]. A jig-shape optimization of an HSCT wing was also performed by Baker and Giesing [7] using aeroelastic design optimization (ADOP) [8] and advanced integrated loads subsystem (AILS) [9] codes. In the study by Baker and Giesing, the takeoff gross weight of the baseline HSCT aircraft was decreased by adjusting the wing jig twist.

The preliminary aerodynamic shape optimization of a candidate low-boom supersonic aircraft configuration, designated as the C607 model, for the desired sonic boom level has been performed by the Lockheed Martin Skunk Works (LMSW) (Palmdale, California) and was used as the starting point for this study. Based on optimum outer-mold-line configuration, a finite element (FE) structural model was created also by LMSW. In this study, jig-shape optimization with the FE structural model is performed to make aeroelastic trim shape as close to the optimum outer-mold-line configuration as possible. This type of decoupled approach has been introduced and applied to the design of a HSCT wing [10].

The primary objective of the current jig-shape optimization study is to minimize error between the aeroelastic trim shape and the optimum outer-mold-line configuration (C607, target trim shape) using a numerical optimization procedure together with a least-squares surface-fitting technique. A mesh regeneration technique for jig-shape optimization is based on a linear combination of basis functions. The least-squares surface-fitting technique is used to compute a starting design configuration of the numerical optimization procedure in the object-oriented optimization (O^3) tool [11, 12, 13].

II. Theoretical Background of the Jig-Shape Optimization Procedure

In this study, the numerical optimization procedure is performed using the O^3 tool developed at the NASA Armstrong Flight Research Center. This O^3 tool has been successfully applied to structural dynamic model tuning [14], aerodynamic model tuning [15], and multidisciplinary design optimization [16, 17] challenges and solutions.

A. Jig-Shape Optimization Problem Statement

For the jig-shape optimization problem, the design jig-shape, $\{jig\}_d$, is defined in Eq. (1),

$$\{jig\}_d \equiv \{jig\}_b + \{\Delta jig\} \tag{1}$$

where $\{jig\}_b$ is the C607 baseline jig-shape and $\{\Delta jig\}$ is assumed in Eq. (2),

$$\{\Delta jig\} = [\boldsymbol{\Phi}]\{X\} \tag{2}$$

where $[\boldsymbol{\Phi}]$ and $\{X\}$ are a basis matrix defined by Eq. (3),

$$[\boldsymbol{\Phi}] = [\{\phi\}_1\{\phi\}_2 \dots \{\phi\}_{ndv}], \tag{3}$$

and a design variable vector, respectively, and ndv is the number of design variables. The vector $\{\phi\}_i$ in Eq. (3) is the i-th basis function. The size of vectors in Eq. (1) is the number of grid points in the FE structural model times three, *ngrid×3*. Based on the design jig-shape, trim analysis is performed and this procedure is symbolized in Eq. (4),

$$\{jig\}_d \xrightarrow[trim\ analysis]{\Longrightarrow} \{T\}_d \tag{4}$$

where $\{T\}_d$ is the trim shape based on the design jig-shape at the surface grids and the size of this vector is the number of surface grid points in the FE structural model times three, *nsurf×3*. Therefore, an unconstrained optimization problem statement is as follows:

Find design variables $\{X\} = \left[X_1, X_2, \dots, X_{ndv}\right]^T$ which minimizes Eq. (5):

objective function:
$$F(X) = \sum_{j=1}^{nsurf\times 3} \Delta T_j{}^2 \tag{5}$$

subjected to Eq. (6):

side constraints:
$$X_i^L \le X_i \le X_i^U \quad i = 1, 2, \dots, ndv \tag{6}$$

where $\{\Delta T\}$ in Eq. (5) is defined in Eq. (7).

$$\{\Delta T\} \equiv \{T\}_t - \{T\}_d \tag{7}$$

The first term, $\{T\}_t$, in Eq. (7) is the target trim shape at the surface grids, and ΔT_j in Eq.(5) is the j-th element of the vector $\{\Delta T\}$. Four analysis modules for the computation of the objective function given in Eq. (5) are described in the following sections.

B. Updated Jig-Shape Module

A design jig-shape during optimization can be updated using Eq. (8) derived by substituting Eq. (2) into Eq. (1).

$$\{jig\}_d \equiv \{jig\}_b + [\mathbf{\Phi}]\{X\} \quad (8)$$

The design jig-shape, $\{jig\}_d$, is created using the baseline jig-shape, $\{jig\}_b$, basis matrix, $[\mathbf{\Phi}]$, and design variable vector, $\{X\}$, using an updated jig-shape module, an in-house shape-change code, as shown in Fig. 1. The design jig-shape saved on the updated grid shape file is represented in the figure. The basis matrix file, $[\mathbf{\Phi}]$, is created before the optimization procedure using an MSC Nastran™ (MSC Software, Newport Beach, California) output file [18] from a modal analysis. The maximum deflection of each basis function, $\{\phi\}_i\ i = 1, 2, \ldots, ndv$, is normalized to one inch. In this study, mode shapes using the baseline jig-shape are selected as basis functions because of the mutual orthogonality of mode shapes. A design variable vector $\{X\}$ (see Eq. (8)) is generated by the O^3 tool (Fig. 1).

C. Modal Analysis Module

Trim analysis using the ZAERO [19] (ZONA Technology, Inc., Scottsdale, Arizona) code requires weight, mass moment of inertias, center of gravity (CG) locations, a system mass matrix for the distributed inertia loads, and rigid-body modes. These elements are obtained using the modal analysis in the MSC Nastran™ modal analysis. Input and output file flows for this module are given in Fig. 2. In this figure, the modal input file represents the MSC Nastran™ input deck, and updated grid shape file is included in this modal input file. Output files from this modal analysis are the modal output file and the system mass matrix file.

D. Trim Analysis Module

In this study, trim analyses are based on the ZAERO code. The trim input file for the ZAERO computer simulation should be updated during the optimization procedure using updated weight, mass moment of inertias, and CG locations, and this update is performed using the update trim input deck module, as shown in Figure 3. Input data for this pre-processor code, an in-house code for updating a trim input deck, are the modal output file and the template input file for ZAERO code, as shown in Fig. 3. Output from this pre-processor code is the trim input file.

A ZAERO computation is performed using the trim input, modal output, and system mass matrix files. A trim deformation from ZAERO code is based on the aerodynamic model. For the objective function computation, trim shape should be based on the FE structural model. Therefore, the external load (aerodynamic load and inertia load) vectors at structural grid locations, external loads file in Fig. 3, are saved for the next static analysis procedure.

E. Objective Function Module

Trim deformation as shown in Fig. 4 is computed using the MSC Nastran™ static analysis with inertia relief. A flow chart of the objective function module is shown in Fig. 5. In this chart, the static input file is the MSC Nastran™ input deck; the updated grid shape and external loads files are included in the static input file. The "Trim deflection" block in Fig. 5 represents the first in-house post-processor code. This program reads the static output file and trim output file and saves the surface grid shape file which is the grid geometry plus deformed shape and trim rotations of the aircraft at all the grid locations.

The "Objective function" block in Fig. 5 represents the second post-processor code. Input data for this post-processor code are the target grid shape and surface grid shape files. The target grid shape file is FE grid geometry information at the surface grids only. The current trim shape at the surface grids, $\{T\}_d$, therefore, is selected from the surface grid shape file and saved in a temporary file. Next, the trim shape error, $\{\Delta T\}$, at the surface grids defined in Eq. (7) is computed. Lastly, the objective function given in Eq. (5) is computed and the result is saved in the objective function file. The O^3 tool reads in the objective function file to continue the optimization procedure. The flow chart of the complete analytical procedure is shown in Fig. 6.

F. Computation of the Starting Design Variables: Using the Least-Squares Surface-Fitting Technique

The trim shape error, $\{\Delta T\}_t$, between the target trim shape, $\{T\}_t$, and the trim shape based on the baseline jig-shape, $\{T\}_b$, at the cruise flight condition is defined in Eq. (9),

$$\{\Delta T\}_t \equiv \{T\}_t - \{T\}_b \quad (9)$$

where the trim shape, $\{T\}_b$, is defined in Eq.(10).

$$\{jig\}_b \xRightarrow[trim\ analysis]{} \{T\}_b \tag{10}$$

First, the *i*-th trim shape, $\{T\}_i$, based on the *i*-th basis functions, $\{\phi\}_i$, is obtained from the trim analysis symbolized in Eq. (11).

$$\{jig\}_b + \{\phi\}_i \xRightarrow[trim\ analysis]{} \{T\}_i \qquad i = 1, 2, \dots, ndv \tag{11}$$

The *i*-th shape function, $\{\Delta T\}_i$, therefore, is defined in Eq. (12).

$$\{\Delta T\}_i \equiv \{T\}_i - \{T\}_b \tag{12}$$

From a matrix $[\boldsymbol{\Psi}]$ in Eq. (13),

$$[\boldsymbol{\Psi}] = [\{\Delta T\}_1 \{\Delta T\}_2 \dots \{\Delta T\}_{ndv}], \tag{13}$$

the trim shape error, $\{\Delta T\}_t$, at the starting configuration can be a linear combination of *ndv* shape functions, $\{\Delta T\}_i$, as shown in Eq. (14).

$$[\boldsymbol{\Psi}]\{X\} = \{\Delta T\}_t \tag{14}$$

The starting design variable vector, $\{X\}$, therefore is computed as shown in Eq. (15).

$$\{X\} = ([\boldsymbol{\Psi}]^T [\boldsymbol{\Psi}])^{-1} [\boldsymbol{\Psi}]^T \{\Delta T\}_t \tag{15}$$

III. Modal and Trim Analyses of the C607 Model

An FE structural model of the C607 model is shown in Fig. 7. The modal analysis is performed using the cruise weight with forward CG configuration. The first ten symmetric flexible frequencies of baseline configuration obtained from the MSC Nastran™ computation are given in Table 1, and the corresponding mode shapes are shown in Fig. 8 and Fig. 9. Lacking a completely symmetric weight distribution, some asymmetric motion is observed among the primarily symmetric modes. For example, the trailing edge of the right stabilator tip, shown in Fig. 8(c), moves more than does the same location on the left stabilator. In this study, these symmetric mode shapes as well as three rigid rotation shapes are used as basis functions, $\{\phi\}_i\ i = 1, 2, \dots, ndv$, of the optimization procedures.

An aerodynamic model of the C607 model for the ZAERO-based trim analysis with 3,673 panels is shown in Fig. 10. The body macro-elements are used for the idealization of the fuselage, engine, and engine nozzle area to have reasonable aerodynamic load distribution with a lifting-surface theory. Airfoil thickness and camber effects of the canard, wing, stabilator, and T-tail are included in this aerodynamic model to increase the accuracy of the lifting-surface theory. Summaries of four trim analyses based on different Mach numbers, altitudes, and CG locations are presented in Table 2. These trim analyses are based on the cruise weight under 1-g level flight configuration. Three trim equations, including translational acceleration along the z axis (Nz), roll acceleration (Pdot), and pitch acceleration (Qdot), together with three trim variables, angle of attack and right and left stabilator deflection angles, are used in these trim analyses. In these trim analyses, roll acceleration, Pdot, trim equation, and different stabilator deflection angles account for asymmetric trim responses. Angle of attack values are near 3 deg, and stabilator deflection angles are between 1.1 deg and 2.4 deg, as shown in Table 2.

Trim results, such as aerodynamic loads, trim deflections, and trim deformations, are based on the aerodynamic model shown in Fig. 10. In this study, trim deflection is defined as trim deformation plus deflection due to rigid rotation as shown in Fig. 4. The jig-shape optimization is based on the FE structural model shown in Fig. 7, therefore, the MSC Nastran™ static analysis with inertia relief is used to compute the trim deformation using aerodynamic and inertia loads obtained from aeroelastic ZAERO computations. The aerodynamic force vectors under case 3 in Table 2 are shown in Fig. 11.

IV. Jig-Shape Optimizations

The jig-shape optimization is performed at Mach 1.42 and altitude of 55,000 ft under 1-g level flight conditions. Aileron and T-tail deflection angles are zero degrees. The cruise weight with forward CG configuration was selected for the jig-shape optimization. In this study, a given C607 FE model with rigid angle of attack and rigid stabilator rotation angles are used to create the target trim shape.

The trim shape error, $\{\Delta T\}_t$, in Eq. (9), before the first optimization procedure, is shown in Fig. 12. In this study, the unconstrained optimization in Eqs. (5), (6), and (7) with the least-squares surface-fitting technique in Eq. (15) is used to minimize the trim shape error. In Fig. 12, the maximum trim shape error is 0.9844 inches at the trailing edge of the wing tip area and the corresponding objective function value in Eq. (5) is 2251. Design variable values, objective function values, and the maximum trim shape error are summarized in Table 3.

A. First Optimization Run

The first ten symmetric flexible modes in Table 1, rigid pitch shape, and rigid left and right stabilator rotation shapes were selected as 13 basis functions in the first optimization run. The starting design variable values were obtained using Eq. (15) and are presented in Table 3 in the column labeled "Optimization #1 Start". The objective function value at the starting configuration is 14.04. A dramatic reduction in objective function value is accomplished using the least-squares surface-fitting technique of Eq. (15).

Next, numerical optimization using the O^3 tool is performed. The optimization results are also presented in Table 3, these in the column labeled "Optimization #1 Optimum". Minor improvement is achieved using numerical optimization: the objective function value changes from 14.04 to 14.02. The trim shape error distribution after the numerical optimization is shown in Fig. 13.

B. Second Optimization Run

As shown in Fig. 13, 13 basis functions for the first optimization run are not enough to fit trim shape errors properly on the canard, T-tail, stabilator, and outboard wing area; the canard and T-tail modes, also given in Table 1 and Figs. 9(e) and 9(f), are also included as the basis functions. Asymmetric stabilator and outboard wing modes as shown in Fig.13, however, are not available within the first 50 flexible modes of the C607 model using the cruise weight with forward CG configuration.

First, starting design variables are computed; these are summarized in Table 3 in the column labeled "Optimization #2 Start". The objective function value is further improved from 14.02 to 6.255 with two additional basis functions. In the next step, numerical optimization using the O^3 tool is performed; the resulting design variables as well as the objective function value and the maximum trim shape error are summarized in Table 3 in the column labeled "Optimization #2 Optimum". The corresponding trim shape error is shown in Fig. 14. The numerical optimization procedure improves the objective function value from 6.255 to 6.232.

C. Third Optimization Run

Asymmetric basis functions and asymmetric trim shape error distribution, Fig. 12, cause asymmetric trim shape error over the canard and T-tail area as shown in Fig. 14. This type of trim shape error is not observed in the mode shapes of the C607 model, and this trim shape error in Fig. 14 is defined as a residual shape in this study. This residual shape is included as the additional basis function for the third optimization run. The 16-th shape function, $\{\Delta T\}_{16}$, is computed using the residual function in Fig. 14 and Eqs. (11) and (12). The new starting design variables are computed using Eq. (15) and summarized in Table 3 in the column labeled "Optimization #3 Start". The objective function value became 0.03269 and the trim shape errors are shown in Fig.15. Numerical optimization was performed, and results are also given in Table 3, these in the column labeled "Optimization #3 Optimum".

Based on the definition of the objective function in Eq. (5), the objective function value at the global optimum point should equal zero. In Table 3, the objective function value after the third numerical optimization run is 0.00917, which is close enough to the global optimum value. The maximum trim shape error after the third numerical optimization run is 0.00367 inch at the trailing edge of the left lower wing tip section. The trim shape errors after the third numerical optimization run are shown in Fig.16. The trim shape errors are further decreased after the numerical optimization run as shown in Figs. 14 and 15. For example, the trim shape errors of 0.00238 inch and 0.00133 inch at the fuselage nose and canard area became 0.00049 inch and 0.00025 inch, respectively, after the numerical optimization.

The final jig-shape configuration is compared with the corresponding starting configuration and results are given in Fig. 17 and Table 4. In Fig. 17, baseline and optimum jig-shapes are plotted using black and blue colors, respectively. It should be noted from Figs. 12 and 17 that trim shape error in Fig. 12 is similar to the difference between

optimum and baseline jig-shape configuration in Fig. 17. For example, -0.989 inch at the trailing edge of the right wing tip section in Fig. 17 is 0.9844 inch in Fig. 12. Similarly, -0.337 inch at the fuselage nose in Fig. 17 is 0.329 inch in Fig. 12. Therefore, subtracting the trim shape error computed before jig-shape optimization from a given finite element model may give a good estimate for the optimum jig-shape configuration.

The angle of attack of the C607 model under baseline and optimum jig-shape configurations is compared in Table 5. Angle-of-attack values based on the both rigid and flexible structural assumptions are provided in this table. The optimum jig-shape configuration based on the rigid-angle-of-attack assumption is also shown in Fig. 18. The angle-of-attack difference using rigid and flexible structural assumption is -0.0409 degree (= 3.0624 – 3.1033) and the distance from the fuselage nose (25.46, 0.0, 82.51) to the center-of-gravity location (836.09, -0.1897, 100.68) is 810.83 inch. Therefore, z deflection due to flexible angle of attack effect is roughly -0.579 inch. Corresponding design variable, design variable number 1, at the end of the third optimization run was -0.5745 as shown in Table 3. It should be noted that the maximum z deflection of the corresponding basis function (rigid angle-of-attack rotation) is assumed to be 1 inch. The jig-shape difference at fuselage nose based on the rigid-angle-of-attack assumption is 0.240 inch as shown in Fig. 18. Therefore, the flexible-angle-of-attack effect, -0.579 inch, is added to 0.240 inch; the jig-shape difference at the fuselage nose based on the-flexible-angle-of-attack assumption then becomes -0.339 inch (-0.337 inch shown in Fig.17). Therefore, flexible angle of attack effect is successfully captured in this study using three rigid rotation basis functions.

After the jig-shape optimization, 12 frequencies for the basis functions are changed negligibly small; these are given in Table 1. The maximum frequency change due to the jig-shape optimization is less than 0.12 percent. The minor changes in mass moment of inertia are presented in Table 4. The effect of the jig-shape changes on the flutter boundaries, structural margin of safety, and buckling load factor might be negligibly small.

V. Conclusion

The jig-shape optimization study in this paper is based on unconstrained optimization. In this study, the jig-shape optimization is performed using the two-step approach. The first step is computing the starting design variables using the least-squares surface-fitting technique. The next step is the fine-tuning of the jig-shape using the numerical optimization procedure. The basis functions are added to the baseline jig-shape so as to have the updated jig-shapes available during the optimization procedure. The symmetric mode shapes from the modal analysis of the cruise weight with forward center-of-gravity configuration are selected as basis functions. A total of 12 mode-shape-based basis functions, basis function for the rigid pitch, and basis functions for the rigid left and right stabilator rotations are used during the second optimization run to fit the trim deformation and flexibility effect on trim variables; however, trim shape error still needs more improvement for acceptable trim shape error distributions. The trim shape error distribution after the second optimization run is selected as the residual shape and this shape is included as an additional basis function. The successful trim shape error distribution is obtained after the third optimization run. The maximum trim shape error is 0.00367 inch at the trailing-edge of the left lower wing tip section.

Table 1. Natural frequencies of the first 12 symmetric flexible modes.

Mode	Frequency (Hz)			Notes
	Baseline	Optimum	% difference	
7	5.634	5.633	-0.02	First fuselage bending
9	9.045	9.032	-0.14	First wing bending + forward fuselage vertical bending + stabilator rotation
11	11.97	11.97	0.00	Forward fuselage vertical bending + first wing bending + stabilator rotation (**Asymmetric**)
15	14.76	14.76	0.00	Stabilator rotation
17	19.23	19.22	-0.05	Wing tip bending + T-tail rotation + flap bending (**Asymmetric**)
19	20.08	20.08	0.00	T-tail rotation (**Asymmetric**)
20	20.54	20.55	0.05	Wing tip bending + T-tail rotation + aileron rotation + flap bending + forward fuselage vertical bending (**Asymmetric**)
22	21.75	21.76	0.05	Aileron rotation + flap rotation + T-tail bending + outboard wing bending torsion
23	22.16	22.16	0.00	Flap rotation + aileron rotation + wing tip bending + T-tail bending (**Asymmetric**)
25	22.70	22.70	0.00	Flap rotation + aileron rotation + T-tail bending (**Asymmetric**)
37	30.79	30.75	-0.13	Canard bending
48	42.96	42.97	0.02	T-tail bending (**Asymmetric**)

Table 2. Trim analysis with cruise weight configuration under different flight conditions and CG locations.

Mode		Case 1	Case 2	Case 3	Case 4
Mach number		1.40	1.40	1.42	1.42
Altitude (ft)		54080	54080	55000	55000
Fuel weight (lb)		18500	18500	18500	18500
Center of gravity location		Forward CG	Aft CG	Forward CG	Aft CG
Maneuver condition		1g level	1g level	1g level	1g level
x acceleration (Nx)		None	None	None	None
y acceleration (Ny)		None	None	None	None
Trim degrees of freedom	Nz (z acceleration)	1g	1g	1g	1g
	Pdot (roll acceleration)	0.0	0.0	0.0	0.0
	Qdot (pitch acceleration)	0.0	0.0	0.0	0.0
Rdot (yaw acceleration)		None	None	None	None
P(roll velocity)		0.0	0.0	0.0	0.0
Q(pitch velocity)		0.0	0.0	0.0	0.0
R(yaw velocity)		0.0	0.0	0.0	0.0
Trim variables	Angle of attack (deg)	**3.011**	**2.911**	**3.104**	**3.002**
	Right stabilator (deg)	**1.290**	**2.039**	**1.092**	**1.870**
	Left stabilator (deg)	**1.586**	**2.333**	**1.481**	**2.265**
Aileron (right=left) (deg)		0.0	0.0	0.0	0.0
Flap (right=left) (deg)		0.0	0.0	0.0	0.0
T-tail (right=left) (deg)		0.0	0.0	0.0	0.0
Canard (right=left) (deg)		0.0	0.0	0.0	0.0
Rudder (deg)		0.0	0.0	0.0	0.0

Table 3. Optimization results.

Design Variable	Baseline	Optimization #1		Optimization #2		Optimization #3		Notes
		Start	Optimum	Start	Optimum	Start	Optimum	
1	0.0	-0.5795	-0.5776	-0.5783	-0.5759	-0.5768	-0.5745	AOA
2	0.0	-1.5063	-1.5078	-1.3482	-1.3489	-1.3427	-1.3440	Stabilator_R
3	0.0	-1.4565	-1.4574	-1.3008	-1.3013	-1.2960	-1.2969	Stabilator_L
4	0.0	0.4108	0.4106	0.4226	0.4228	0.4215	0.4216	Mode 7
5	0.0	-1.0492	-1.0495	-1.0585	-1.0587	-1.0555	-1.0559	Mode 9
6	0.0	0.2851	0.2848	0.2544	0.2541	0.2533	0.2533	Mode 11
7	0.0	1.2202	1.2190	1.0823	1.0814	1.0775	1.0762	Mode 15
8	0.0	.04660	.04569	.00555	.00513	.00525	.00499	Mode 17
9	0.0	0.1273	0.1275	0.1242	0.1243	0.1238	0.1238	Mode 19
10	0.0	.05808	.05803	.02061	.02058	.02061	.02041	Mode 20
11	0.0	-.02754	-.02746	-.04842	-.04848	-.04840	-.04836	Mode 22
12	0.0	-.00712	-.00697	-.02884	-.02907	-.02909	-.02898	Mode 23
13	0.0	0.1212	0.1211	0.1055	0.1056	0.1049	.1050	Mode 25
14	0.0			0.2174	0.2172	0.2161	0.2161	Mode 37
15	0.0			-.07665	-.07671	-.07589	-.07605	Mode 48
16	0.0					-1.002	-1.002	Residual
Maximum error (inch)	0.9844	0.1896	0.1904	.0897	.0905	.00396	.00367	
Objective function value	**2251.**	**14.04**	**14.02**	**6.255**	**6.232**	**.03269**	**.00917**	

Table 4. Cruise weight summary of the C607 model under baseline and optimum jig-shape configurations.

	Baseline	Optimum	% difference
Weight (lb)	18500	18500	0.00
X-C.G. (inch)	836.09	836.09	0.00
Y-C.G. (inch)	-0.18966	-0.18970	0.02
Z-C.G. (inch)	100.68	100.68	0.00
I_{XX}	42680000	42730000	0.12
I_{YX}	-251150	-251008	-0.06
I_{YY}	629920000.	629910000.	0.00
I_{ZX}	-17221000	-17658000.	2.54
I_{ZY}	23158	23070	-0.38
I_{ZZ}	661920000	661890000.	0.00

Table 5. Angle of attack of the C607 model under baseline and optimum jig-shape configurations

Structural assumption	Baseline (degree)	Optimum (degree)
Rigid	3.0624	3.0624
Flexible	3.1036	3.1033

Figures

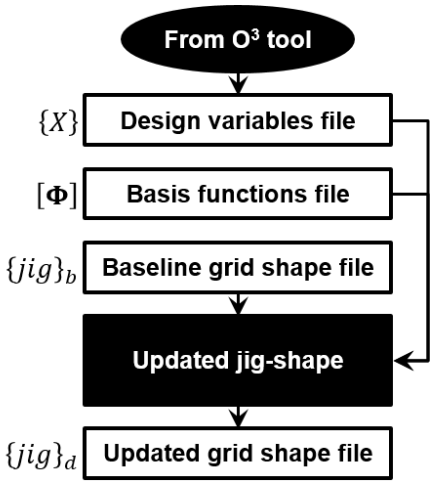

Fig. 1. Updated jig-shape module.

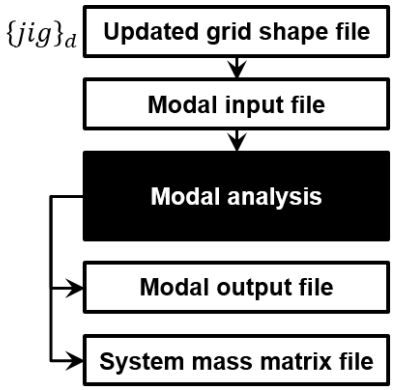

Fig. 2. Modal analysis module.

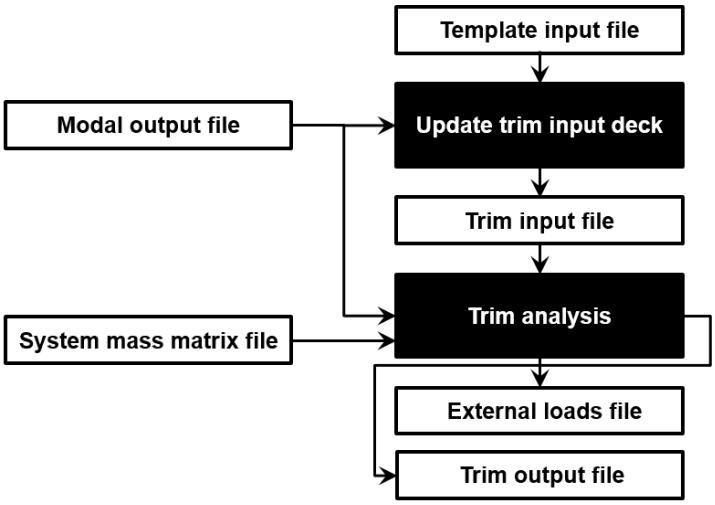

Fig. 3. Trim analysis module.

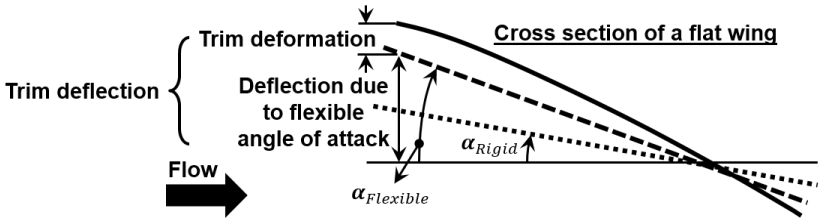

Fig. 4. Definitions of trim deflection and deformation and rigid and flexible angle of attacks

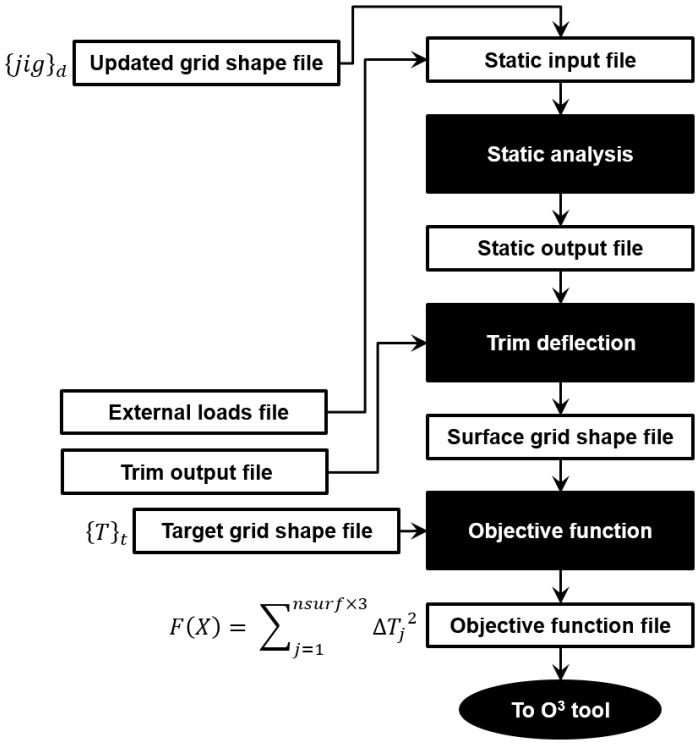

Fig. 5. Objective function module.

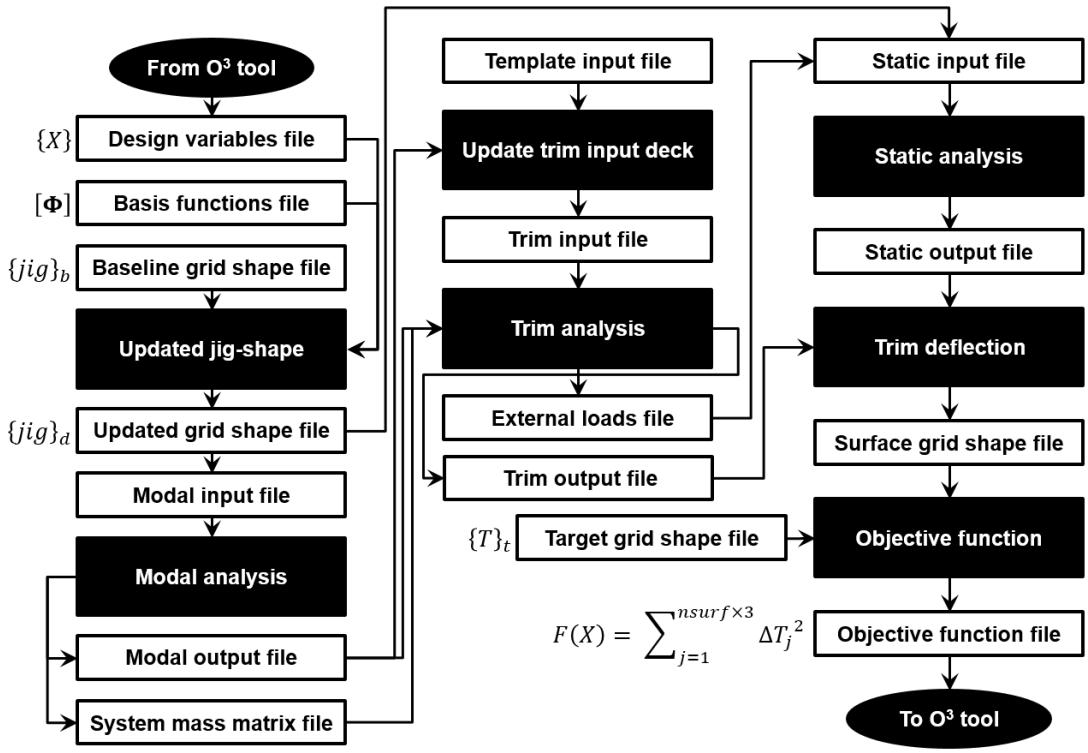

Fig. 6. Complete flow chart of analysis modules.

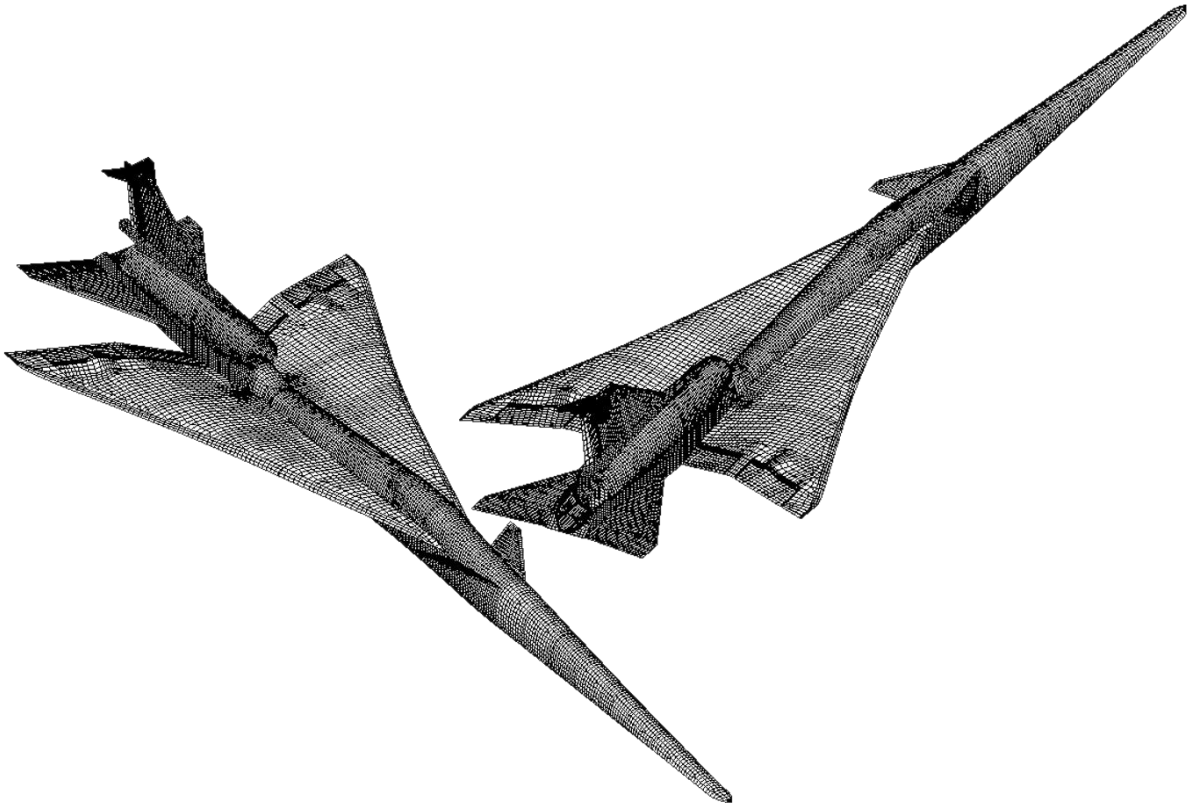

Fig. 7. Finite element structural model of C607 model.

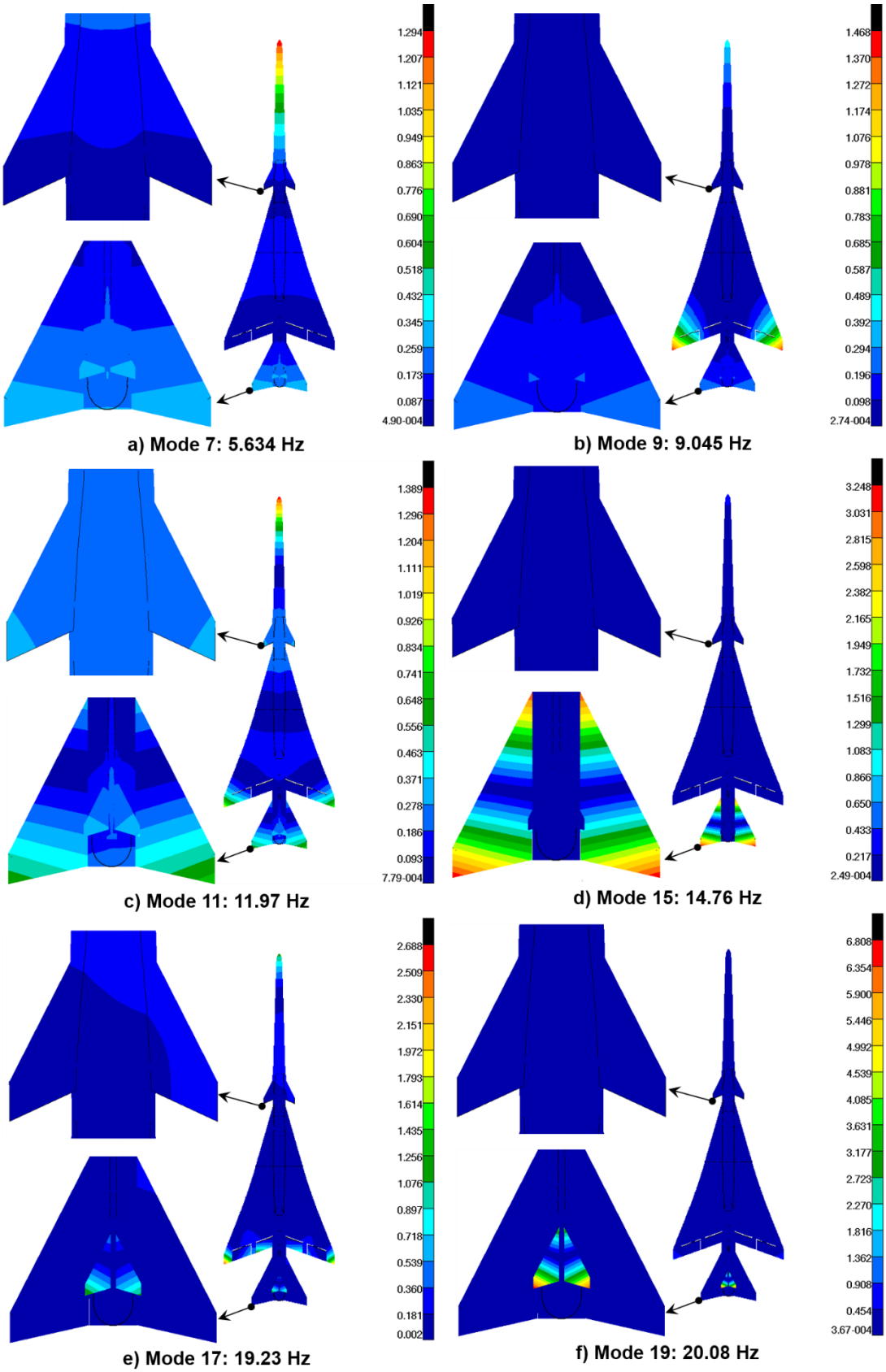

Fig. 8. Symmetric flexible modes 7, 9, 11, 15, 17, and 19.

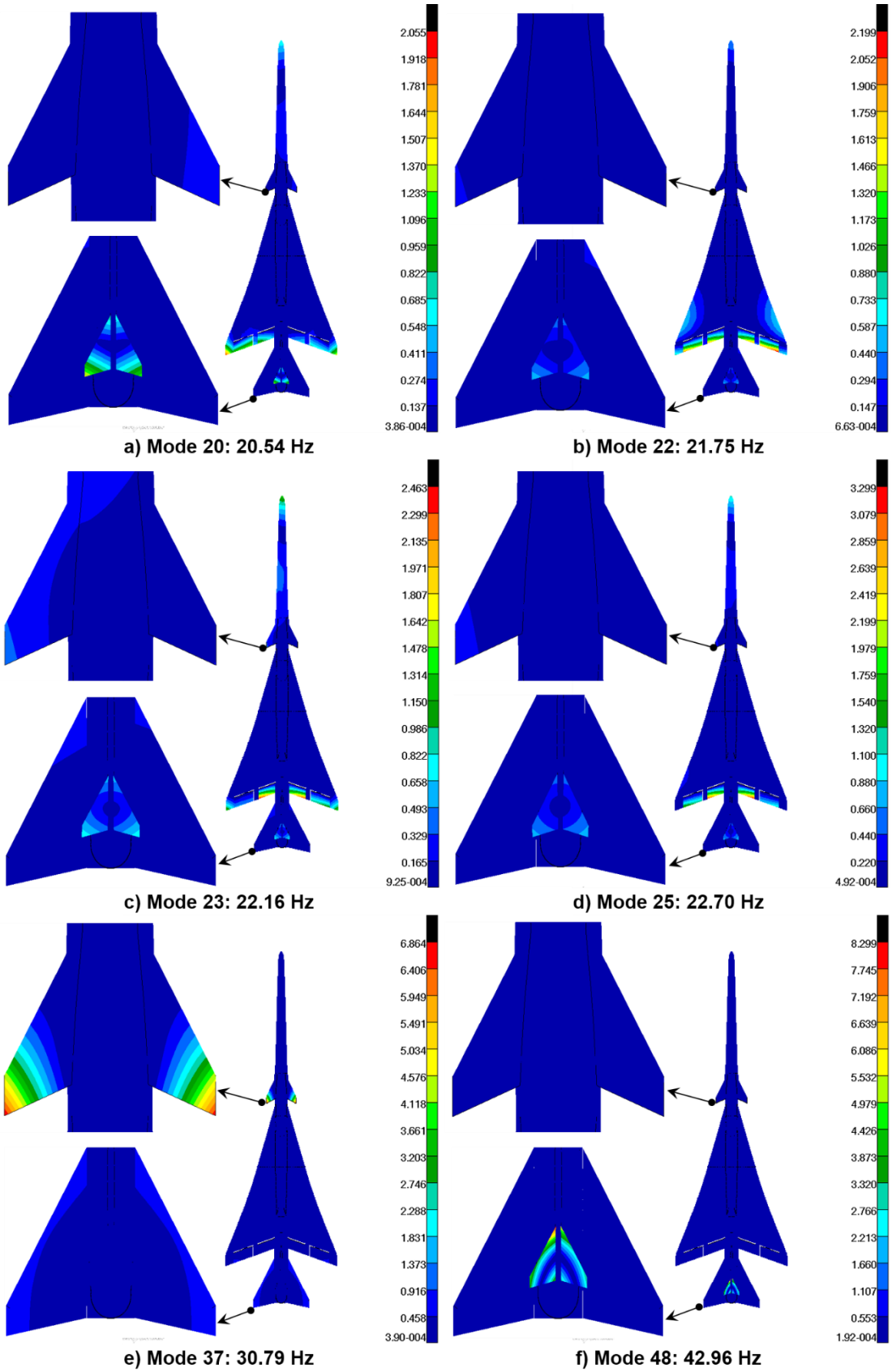

Fig. 9. Symmetric flexible modes 20, 22 23, 25, 37, and 48.

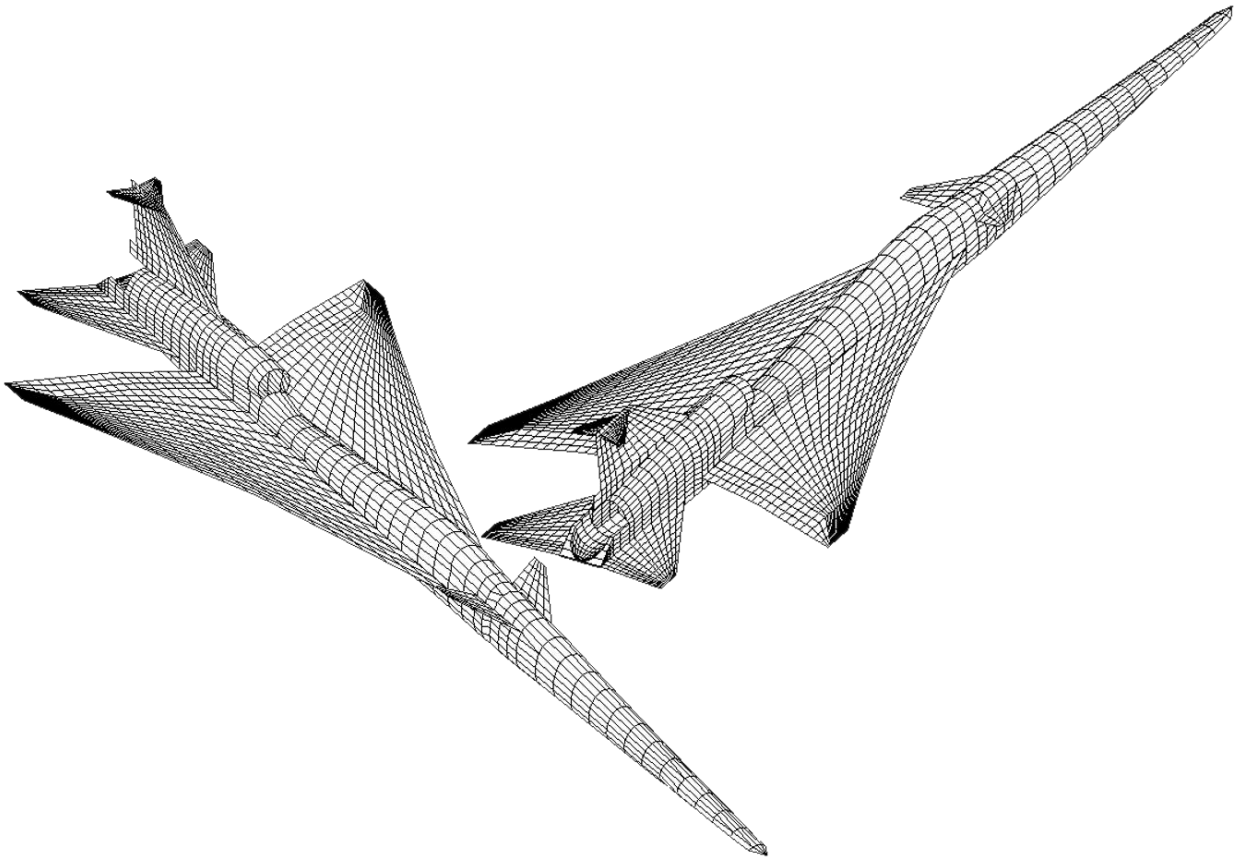

Fig. 10. Aerodynamic model of the C607 model.

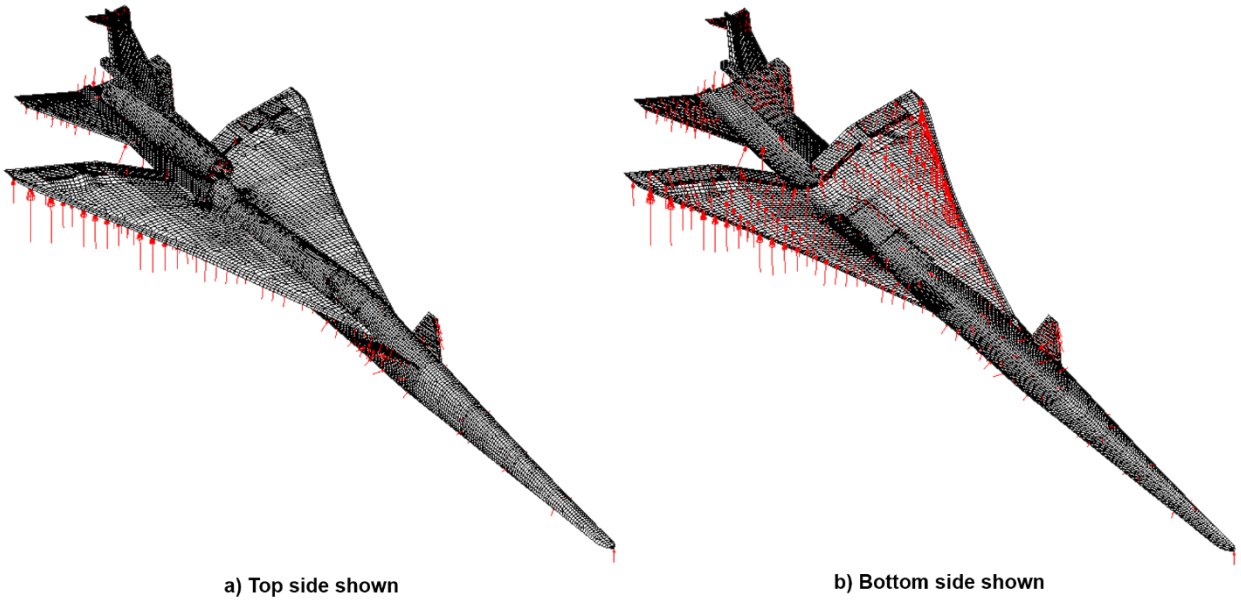

Fig. 11. Aerodynamic force vectors acting on the structural C607 model.

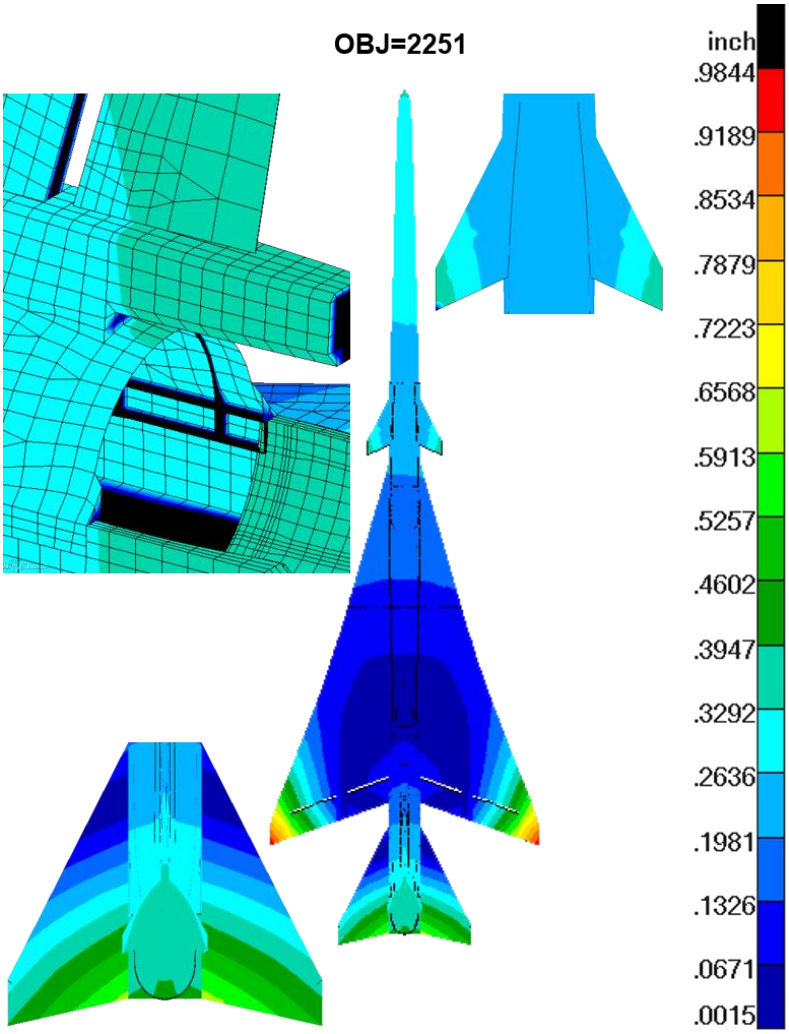

Fig. 12. Trim shape error before the first optimization run.

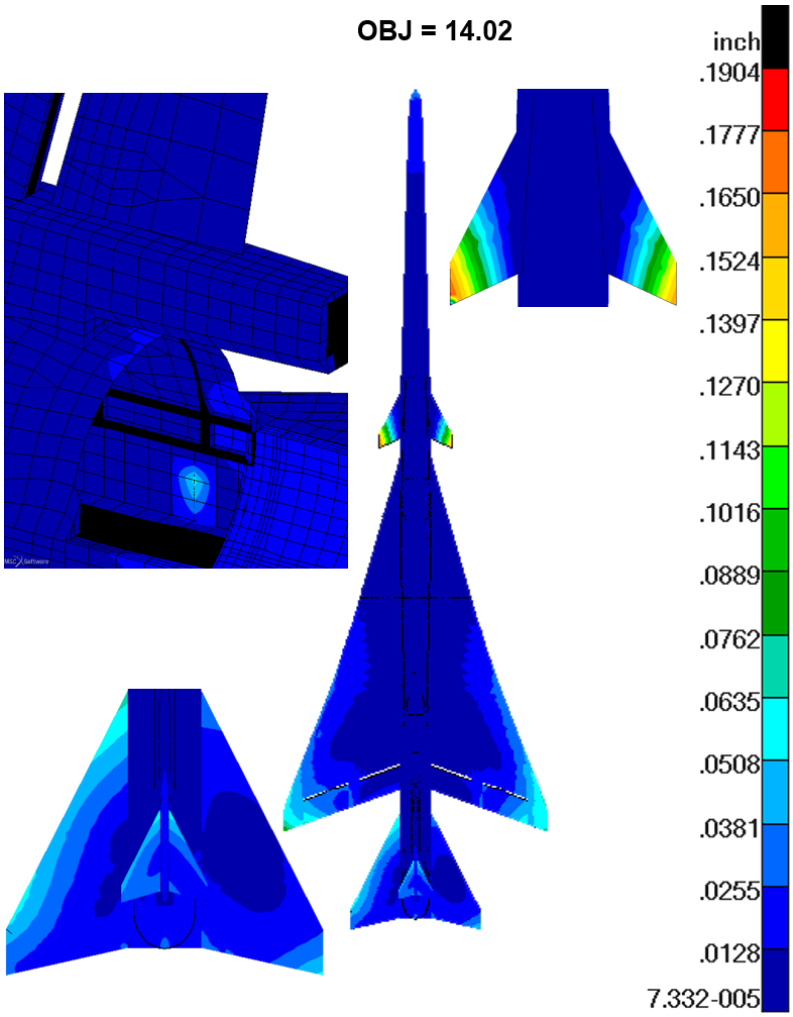

Fig. 13. Trim shape error after the first optimization run.

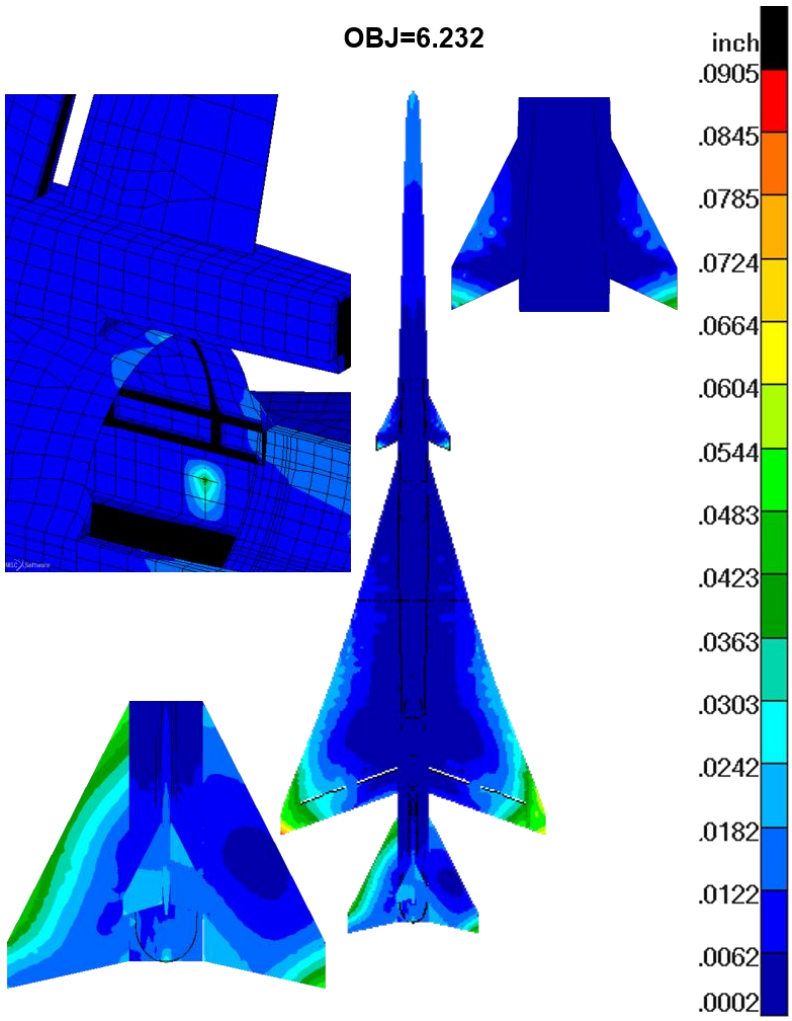

Fig. 14. Trim shape error after the second optimization run.

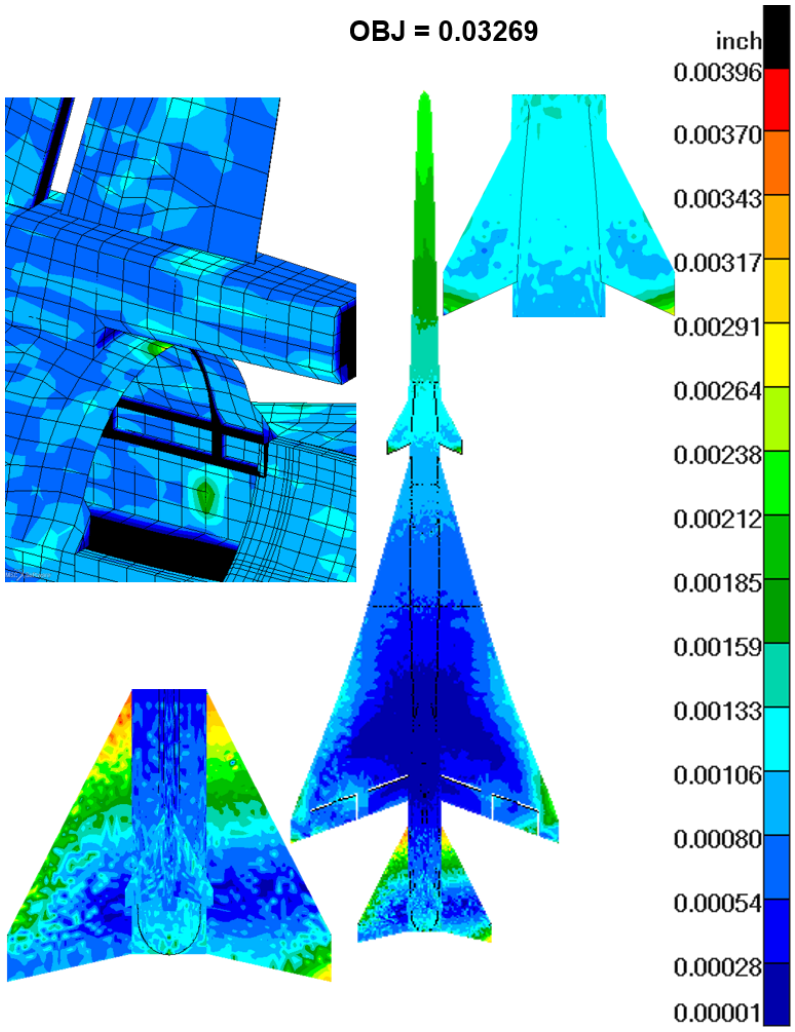

Fig. 15. Trim shape error after using the third least squares surface fitting technique.

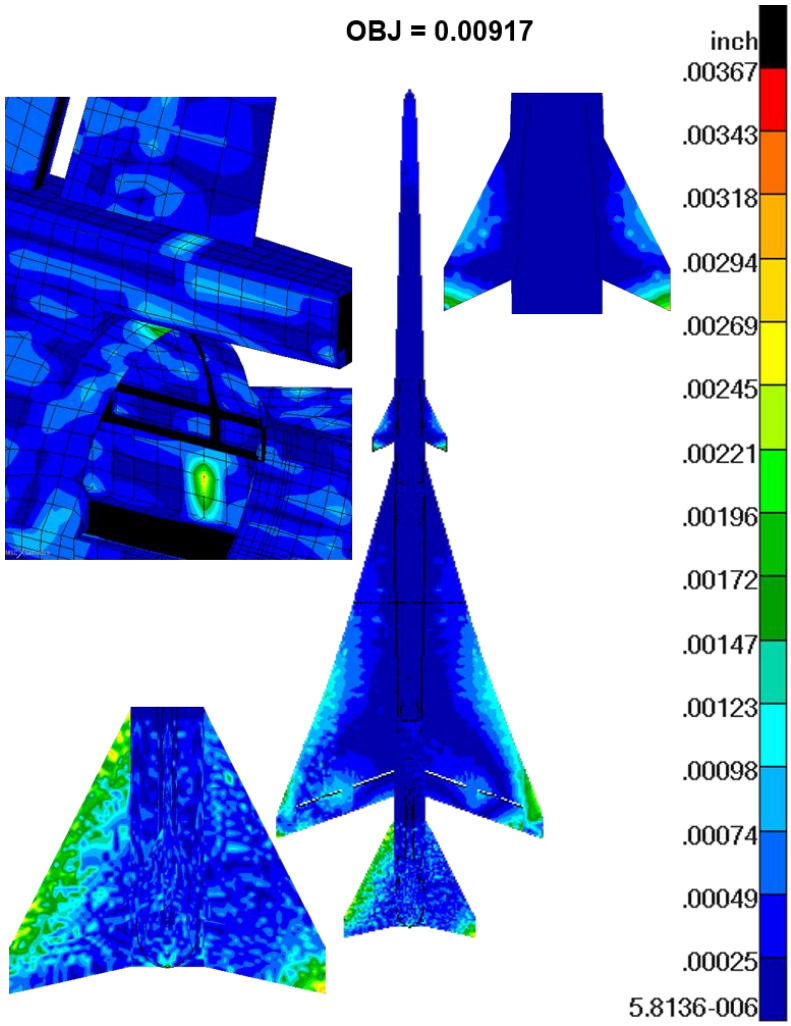

Fig. 16. Trim shape error after the third optimization run.

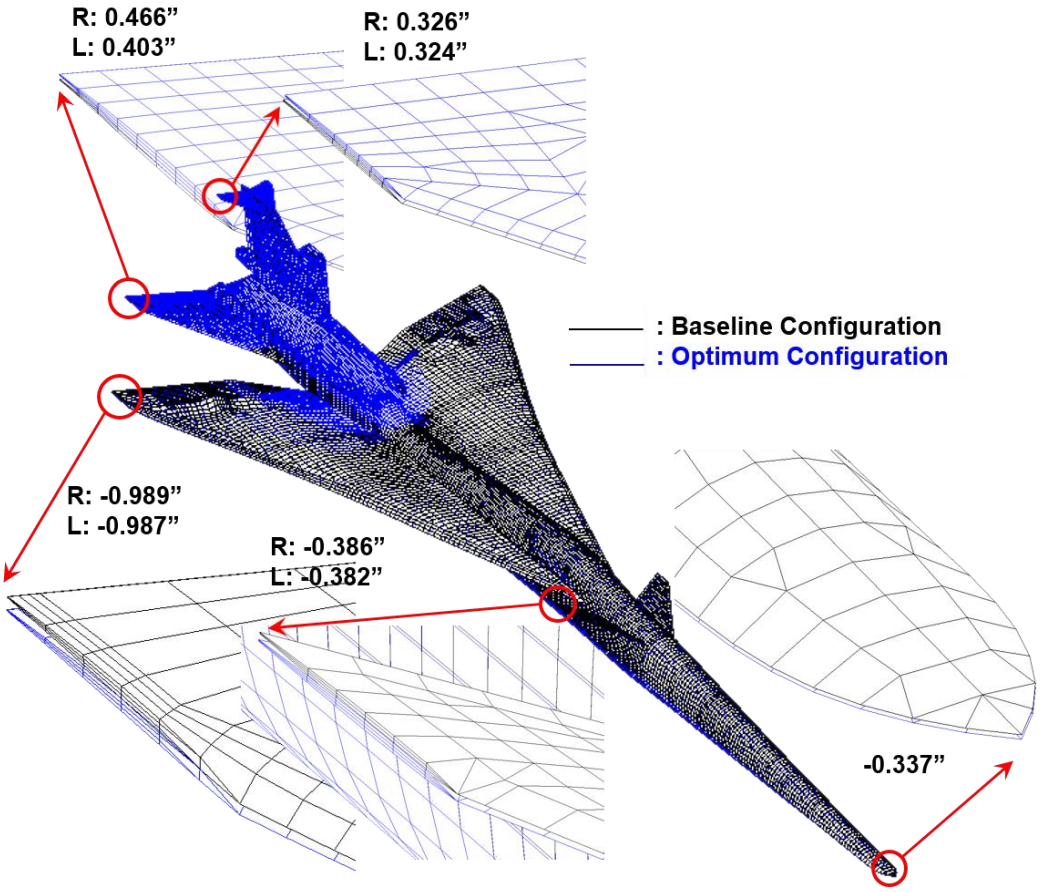

Fig. 17. Optimum jig-shape configuration with rigid rotation modes.

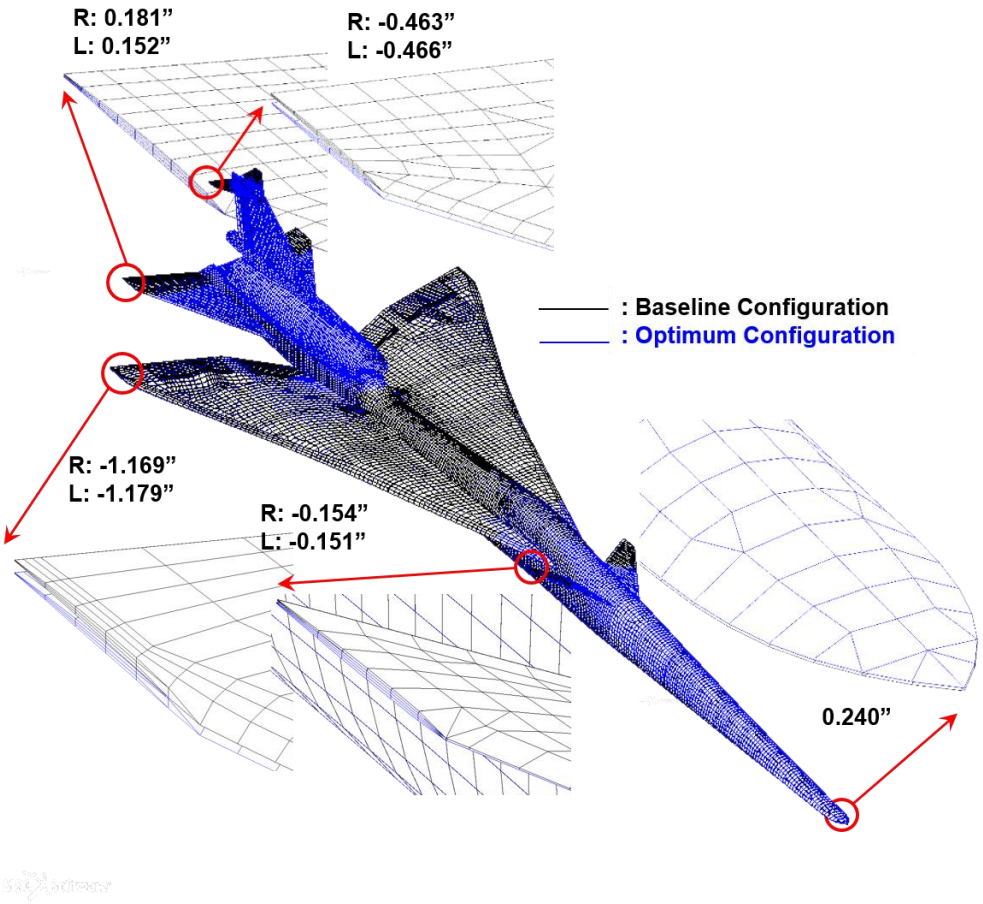

Fig. 18. Optimum jig-shape configuration without rigid rotation modes.

References

[1]Bhatia, K. G., and Wertheimer, J., “Aeroelastic Challenges for a High Speed Civil Transport,” AIAA-93-1478, April 1993. doi: 10.2514/6.1993-1478

[2]Ordaz I., Geiselhart, K. A., and Fenbert, J. W., “Conceptual Design of Low-Boom Aircraft with Flight Trim Requirement,” *Journal of Aircraft*, Vol. 52, No. 3, 2015, pp. 932-939. http://dx.doi.org/10.2514/1.C033160

[3]Sobieszczanski-Sobieski, J., and Haftka ,R. T., “Multidisciplinary Aerospace Design Optimization: Survey of Recent Developments,” AIAA 96-0711, January 1996. doi: 10.2514/6.1996-711

[4]Rohl, P. J., Mavris, D. N., and Schrage, D. P., “Combined Aerodynamic and Structural Optimization of High-Speed Civil Transport Wing,” AIAA 95-1222, April 1995. doi: 10.2514/6.1995-1222

[5]Carlson, H. W., Chu, J., Ozoroski, L. P., and McCullers, L. A., “Guide to AERO2S and WINGDES Computer Codes for Prediction and Minimization of Drag Due to Lift,” NASA TP-3637, 1997.

[6]Neill, D. J., Johnson, E. H., and Canfield, R., “ASTROS - A Multidisciplinary Automated Structural Design Tool,” *Journal of Aircraft*, Vol. 27, No. 12, 1990, pp. 1021-1027. doi: 10.2514/6.1987-713

[7]Baker, M., and Giesing, J., “A Practical Approach to MDO and its Application to an HSCT Aircraft,” AIAA 95-3885, September 1995. doi: 10.2514/6.1995-3885

[8]Tzong, T. J., Sikes, G. D., and Loikkanen, M. J., “Multidisciplinary Design Optimization of a Large Transport Aircraft Wing,” AIAA 92-1002, February 1992. doi: 10.2514/6.1992-1002

[9]D’Vari, R. and Baker, M., “A Static and Dynamic Aeroelastic Loads and Sensitivity Analysis for Structural Loads Optimization and Its Application to Transport Aircraft,” AIAA 93-1643, April 1993. doi: 10.2514/6.1993-1643

[10]Aly, S., Ogot, M., Pelz, R., and Siclari, M., “Jig-Shape Static Aeroelastic Wing Design Problem: A Decoupled Approach,” *Journal of Aircraft*, Vol. 39, No. 6, 2002, pp. 1061-1066. doi: 10.2514/2.3035

[11]Pak, C-g., “Preliminary Development of an Object-Oriented Optimization Tool,” NASA/TM-2011-216419, 2011.

[12]Pak, C-g. and Truong, S. S., “Extension of an Object-Oriented Optimization Tool: User’s Reference Manual,” NASA/TM-2015-218733, 2015.

[13]National Aeronautics and Space Administration, "Optimization Tool Integrates Software to Automate Design Process," https://www.nasa.gov/offices/ipp/centers/dfrc/technology/DRC-010-013-O3-Tool.html [retrieved 5 October 2017].
[14]Pak, C-g. and Truong, S., "Creating a Test-Validated Finite-Element Model of the X-56A Aircraft Structure," *Journal of Aircraft*, Vol. 52, No. 5, 2015, pp. 1644-1667. doi: 10.2514/1.C033043
[15]Pak, C-g., "Unsteady Aerodynamic Model Tuning for Precise Flutter Prediction," *Journal of Aircraft*, Vol. 48, No. 6, 2011, pp. 2178-2184. doi: 10.2514/1.C031495
[16]Li, W. W., and Pak, C.-g., "Mass Balancing Optimization Study to Reduce Flutter Speeds of the X-56A Aircraft," *Journal of Aircraft*, Vol. 52, No. 4, 2015, pp. 1359-1365. doi: 10.2514/1.C033044
[17]Pak, C-g., "Aeroelastic Tailoring Study of an N+2 Low-boom Supersonic Commercial Transport Aircraft," AIAA 2015-2791, June 2015. doi: 10.2514/6.2015-2791
[18]*MSC Nastran 2005 Quick Reference Guide*, The MacNeal-Schwendler Corporation, Newport Beach, California, 2005.
[19]*ZAERO User's Manual Version 8.5,* ZONA Technology, Inc., Scottsdale, Arizona, 2011.